Journal of Computational Physics 229 (2010) 301–312

Contents lists available at ScienceDirect

Journal of Computational Physics

journal homepage: www.elsevier.com/locate/jcp

A variational multiscale method for turbulent flow simulation with adaptive large scale space

Volker John [a,b,*], Adela Kindl [c,1]

[a] Weierstrass Institute for Applied Analysis and Stochastics (WIAS), Mohrenstr. 39, 10117 Berlin, Germany
[b] Free University of Berlin, Department of Mathematics and Computer Science, Arnimallee 6, 14195 Berlin, Germany
[c] FR 6.1 – Mathematik, Universität des Saarlandes, Postfach 15 11 50, 66041 Saarbrücken, Germany

ARTICLE INFO

Article history:
Received 7 May 2009
Received in revised form 17 September 2009
Accepted 22 September 2009
Available online 8 October 2009

Keywords:
Variational multiscale method
Turbulent flows
Finite element method
Large scale space
Adaptivity

ABSTRACT

In turbulent flows it is only feasible to simulate large flow structures. Variational multiscale (VMS) methods define these flow structures by projections onto appropriate function spaces. This paper presents a finite element VMS method which chooses the large scale projection space adaptively. The adaption controls the influence of an eddy viscosity model and it is based on the size of the so-called resolved small scales. The adaptive procedure is described in detail. Numerical studies at a turbulent channel flow and a turbulent flow around a cylinder are presented. It is shown that the method selects the large scale space in a reasonable way and that appropriately chosen parameters improve the results compared to the basic method, which uses the same local large scale space in the whole domain and for all times.

© 2009 Elsevier Inc. All rights reserved.

1. Introduction

Incompressible flows are governed by the incompressible Navier–Stokes equations which, in dimensionless form and for no-slip boundary conditions, read

$$\begin{aligned} &\mathbf{u}_t - 2\nu\nabla\cdot\mathbb{D}(\mathbf{u}) + (\mathbf{u}\cdot\nabla)\mathbf{u} + \nabla p = \mathbf{f} \text{ in } (0,T]\times\Omega,\\ &\nabla\cdot\mathbf{u} = 0 \text{ in } [0,T]\times\Omega,\\ &\mathbf{u} = \mathbf{0} \text{ in } [0,T]\times\partial\Omega,\\ &\mathbf{u}(0,\mathbf{x}) = \mathbf{u}_0 \text{ in } \Omega,\\ &\int_\Omega p\, d\mathbf{x} = 0, \text{ in } (0,T]. \end{aligned} \tag{1}$$

Here, $\Omega\subset\mathbb{R}^3$ is a bounded, connected domain with polyhedral boundary $\partial\Omega$, $[0,T]$ is a finite time interval, $\mathbf{u}$ is the fluid velocity, p is the pressure, $\mathbf{f}$ is an external force, ν is the kinematic viscosity, $\mathbf{u}_0$ is the initial velocity field, and $\mathbb{D}(\mathbf{u}) = (\nabla\mathbf{u} + (\nabla\mathbf{u})^T)/2$ is the velocity deformation tensor (symmetric part of the gradient).

Turbulent flows are characterized by a multitude of different sizes for the flow scales, fact which makes the simulation of such flows by direct discretizations generally infeasible with the currently available computer hardware. As the resolution of

* Corresponding author. Address: Weierstrass Institute for Applied Analysis and Stochastics (WIAS), Mohrenstr. 39, 10117 Berlin, Germany. Tel.: +49 30 20372 561; fax: +49 30 2044975.
E-mail addresses: john@wias-berlin.de (V. John), adela@c-kindl.de (A. Kindl).
[1] The research was supported by the Deutsche Forschungsgemeinschaft (DFG), Grants Nos. Jo 329/7-1 and Jo 329/7-2.

0021-9991/$ - see front matter © 2009 Elsevier Inc. All rights reserved.
doi:10.1016/j.jcp.2009.09.025

all flow scales is not possible, and the unresolved scales are important for the turbulent character of the flow, their influence onto the resolved scales needs to be taken into account via a turbulence model.

Popular methods for simulating turbulent flows include $k-\varepsilon$ models [1] and large eddy simulation (LES), see for example [2,3]. In LES, the flow field is decomposed through spatial filtering and this method aims at an accurate simulation of only the so-called resolved scales. Widely used traditional LES models are Smagorinsky-type models [4–6].

As an alternative, variational multiscale (VMS) methods are a rather new approach for simulating turbulent flows. The basic idea of VMS methods, in contrast to traditional LES, is the use of variational projections instead of filtering for the scale decomposition, thus eliminating several difficulties of the traditional LES, e.g. commutation errors [7–10]. VMS methods for turbulent flow simulations were derived from general principles for treating multiscale phenomena [11,12]. For an introduction to as well as a review of VMS methods and their relation and differences to traditional LES methods, we refer to [13–15]. There are meanwhile several realizations of VMS methods, see the reviews in [16–18].

The present paper considers a three-scale VMS method, i.e. the flow is decomposed into three scales: large (resolved) scales, resolved small scales, and (small) unresolved scales. Assuming that the direct influence of the unresolved scales onto the large scales is negligible, and thus the direct influence of the unresolved scales is confined to the resolved small scales, the influence of the unresolved scales onto the resolved small scales is modeled with a turbulence model of eddy viscosity type. There is no direct turbulence modeling for the large scales, however the large scales are still influenced indirectly by the unresolved scales due to the coupling of all three scales.

The considered VMS method uses finite elements as underlying spatial discretization, therefore it is called finite element VMS (FEVMS) method. The projection for the definition of the scales is contained explicitly in the set of equations, see [19] for the first presentation and [20] for a preliminary version of this projection-based FEVMS method. Its parameters are the finite element spaces used to define the scale decomposition and the turbulence model acting directly only on the resolved small scales. Regarding the turbulence model, the parameter in the additional viscous term added to the momentum equation is generally chosen to be an eddy viscosity model of Smagorinsky type [17–19,21]. Regarding the spaces, standard finite element spaces for the incompressible Navier–Stokes equations are used for all resolved scales and the separation of the large and the resolved small scales is achieved through an additional tensor-valued large scale space.

Available numerical studies [17,18,21] show that the choice of the additional large scale space has more influence on the results than changing the parameter in the eddy viscosity turbulence model. All these studies used globally uniform large scale spaces, i.e. the polynomial degree of the finite element tensors was the same for all mesh cells. This polynomial degree was chosen before starting the computations and it remained fixed during the simulations of the flows.

This paper introduces an extension of the projection-based FEVMS method which chooses the large scale space a posteriorly and adaptively. To our best knowledge, the idea of adaptively choosing the large scale space seems to be new. Our aim here is to give a first presentation and first numerical results for this adaptive approach.

The advantages of the adaptive method consist in the fact that, firstly, it is no longer necessary to choose a large scale space for the whole simulation, the new method computes an appropriate large scale space during the simulation. Secondly, the large scale space may change. This property is of importance if main features of the flow field change during the simulation. And thirdly, the large scale space is no longer uniform, different mesh cells may have finite element tensors with different polynomial degree. This feature of the new method takes into account the fact that in general the flow is not equally turbulent in the whole domain. There are subregions, e.g. at walls, with a strong turbulent character and in other subregions the flow behaves more or less laminar. With respect to the large scale space in the projection-based FEVMS method, the first situation corresponds to the necessity of using a locally small large scale space which allows a stronger influence of the eddy viscosity turbulence model. The second situation is vice versa.

The remainder of the paper is organized as follows: Section 2 introduces the considered projection-based FEVMS method. The adaptive algorithm for choosing the large scale space is described in detail in Section 3. A turbulent channel flow and a turbulent flow around a cylinder are studied in Section 4. Finally, Section 5 contains the summary of this paper.

2. Projection-based finite element variational multiscale methods

In the projection-based FEVMS method, all resolved scales belong to standard finite element spaces and an additional large scale space is needed for the scale separation. The resolved scales are decomposed into large and small ones with the help of a projection into the additional large scale space. The FEVMS method presented here contains this projection explicitly as an additional equation.

Let $V^h \times Q^h$ be a pair of inf–sup stable, conforming finite element spaces for the velocity and pressure. Consider an additional finite dimensional space of symmetric 3×3 tensor-valued functions $L^H \subset \{\mathbb{L} \in (L^2(\Omega))^{3\times 3}, \mathbb{L}^T = \mathbb{L}\}$ representing a coarse or large scale space, and let ν_T be a non-negative function representing the turbulent viscosity. The semi-discrete (continuous in time) projection-based FEVMS method with parameters ν_T and L^H then seeks $\mathbf{u}^h : [0,\ T] \to V^h$, $p^h : (0,\ T] \to Q^h$, and $\mathbb{G}^H : [0,\ T] \to L^H$ such that

$$
\begin{aligned}
&(\mathbf{u}_t^h,\ \mathbf{v}^h) + (2\nu\mathbb{D}(\mathbf{u}^h),\ \mathbb{D}(\mathbf{v}^h)) + ((\mathbf{u}^h\cdot\nabla)\mathbf{u}^h,\ \mathbf{v}^h) - (p^h,\ \nabla\cdot\mathbf{v}^h) + (\nu_T(\mathbb{D}(\mathbf{u}^h) - \mathbb{G}^H),\ \mathbb{D}(\mathbf{v}^h)) = (\mathbf{f},\ \mathbf{v}^h), \quad \forall \mathbf{v}^h \in V^h,\\
&(q^h,\ \nabla\cdot\mathbf{u}^h) = 0, \quad \forall q^h \in Q^h,\\
&(\mathbb{D}(\mathbf{u}^h) - \mathbb{G}^H,\ \mathbb{L}^H) = 0, \quad \forall \mathbb{L}^H \in L^H.
\end{aligned}
\tag{2}
$$

The tensor $\mathbb{G}^H$ is the L^2-projection of $\mathbb{D}(\mathbf{u}^h)$ into the large scale space L^H, representing the large scales of $\mathbb{D}(\mathbf{u}^h)$. Consequently, $\mathbb{D}(\mathbf{u}^h) - \mathbb{G}^H$ represents the resolved small scales. The additional viscous term $(\nu_T(\mathbb{D}(\mathbf{u}^h) - \mathbb{G}^H),\ \mathbb{D}(\mathbf{v}^h))$, introduced by the projection-based FEVMS method in the momentum equation, acts directly only on the resolved small scales, which is a main feature of three-scale VMS methods.

A crucial issue for the results obtained with a projection-based FEVMS method of form (2) is the choice of the large scale space $L^H \subseteq \{\mathbb{D}(\mathbf{v}^h) : \mathbf{v}^h \in V^h\}$. Since L^H has been used to distinguish between resolved small scales and large scales, with L^H representing the large scales, it must be in some sense a coarse finite element space. One way of achieving this is by choosing L^H to be a lower order finite element space than V^h on the same grid, called one-level method. This requires that V^h is in some sense a higher order finite element space. An alternative consists in defining L^H on a coarser grid, see [22] for a discussion on one-level and two-level projection-based FEVMS methods. In the present paper, the one-level approach will be used.

The projection terms in (2) can be treated explicitly or implicitly in time. We will restrict here to the implicit treatment, see [21] for comments on the explicit approach. The fully implicit projection-based FEVMS method, discretized in time using a θ-scheme, reads: Find $(\mathbf{u}_k^h, p_k^h, \mathbb{G}_k^H) \in V^h \times Q^h \times L^H$ such that

$$
\begin{aligned}
&(\mathbf{u}_k^h,\ \mathbf{v}^h) + \theta_1 \Delta t_k \big[((2\nu + \nu_{T,k})\mathbb{D}(\mathbf{u}_k^h),\ \mathbb{D}(\mathbf{v}^h)) + ((\mathbf{u}_k^h \cdot \nabla)\mathbf{u}_k^h,\ \mathbf{v}^h) - (\nu_{T,k}\mathbb{G}_k^H,\ \mathbb{D}(\mathbf{v}^h))\big] - (p_k,\ \nabla \cdot \mathbf{v}^h) \\
&\quad = (\mathbf{u}_{k-1}^h,\ \mathbf{v}^h) - \theta_2 \Delta t_k \big[((2\nu + \nu_{T,k-1})\mathbb{D}(\mathbf{u}_{k-1}^h),\ \mathbb{D}(\mathbf{v}^h)) + ((\mathbf{u}_{k-1}^h \cdot \nabla)\mathbf{u}_{k-1}^h,\ \mathbf{v}^h) \\
&\quad -(\nu_{T,k-1}\mathbb{G}_{k-1}^H,\ \mathbb{D}(\mathbf{v}^h))\big] + \theta_3 \Delta t_k (\mathbf{f}_{k-1},\ \mathbf{v}^h) + \theta_4 \Delta t_k (\mathbf{f}_k,\ \mathbf{v}^h), \quad \forall \mathbf{v}^h \in V^h, \\
&0 = (q^h,\ \nabla \cdot \mathbf{u}_k^h), \quad \forall q^h \in Q^h, \\
&0 = (\mathbb{D}(\mathbf{u}_k^h) - \mathbb{G}_k^H,\ \mathbb{L}^H), \quad \forall \mathbb{L}^H \in L^H,
\end{aligned}
\tag{3}
$$

with $\Delta t_k = t_k - t_{k-1}$. We will use in our studies the Crank–Nicolson scheme, $\theta_1 = \theta_2 = \theta_3 = \theta_4 = 0.5$, since this scheme has been proven to be a good compromise between accuracy and efficiency [23,24].

For the main features of an efficient implementation of the fully implicit approach we refer to [19].

3. The projection-based finite element variational multiscale method with an adaptively chosen large scale space

The projection-based FEVMS method requires the choice of the tensor-valued large scale space L^H in order to define the projection. In [19], it has been shown that an efficient implementation of the one-level method requires this space to consist of discontinuous functions. This is also understandable from the fact that the resolved small scales are the projection of an already discontinuous function, namely the deformation tensor of the finite element velocity. In [17–19,21] numerical studies were performed for $L^H = P_0$ and $L^H = P_1^{\text{disc}}$. In the large-space-adaptive FEVMS method, L^H is allowed to posses different polynomial degrees on different mesh cells. The more turbulence a region presents, the stronger the influence of the turbulence model should be and the local polynomial degree of L^H should increase as the amount of turbulence decreases. In regions with strong turbulence, e.g. along the boundary of the domain, a turbulence model is necessary, often in contrast to the interior of the domain.

The local amount of turbulence is given by the local unresolved scales. But these scales are not computable. In the FEVMS method with adaptive large scale space, the amount of turbulence, and in consequence the local polynomial degree of L^H, will be controlled a posteriorly by the local L^2-norm of the resolved small scales $\mathbb{D}(\mathbf{u}^h) - \mathbb{G}^H$. The assumption behind this choice for the local indicator of the amount of turbulence is that the local turbulence intensity is reflected by the size of the local resolved small scales. In other words, if there are many resolved small scales in a subregion, we expect that there are also many scales of the next smaller size, i.e. many unresolved scales, in this subregion. And vice versa, if there are few resolved small scales in a subregion, we expect that in this subregion the amount of unresolved scales is also small.

In order to obtain information on the amount of turbulence, the size of the local resolved small scales

$$
\eta_K = \frac{\|\mathbb{D}(\mathbf{u}^h) - \mathbb{G}^H\|_{L^2(K)}}{\|1\|_{L^2(K)}} = \frac{\|\mathbb{D}(\mathbf{u}^h) - \mathbb{G}^H\|_{L^2(K)}}{|K|^{1/2}}, \quad K \in \mathcal{T}^h,
\tag{4}
$$

where K is a mesh cell of the triangulation $\mathcal{T}^h$, is compared to a mean resolved small scale size. The size of the resolved small scales does not depend on the volume $|K|$ of the mesh cells, with definition (4) the volume of the mesh cells scales out. In cells where the size of the resolved small scales η_K is (very) large compared with the mean resolved small scale size, high turbulence is expected, whereas in cells where η_K is smaller than the mean, the amount of turbulence is estimated to be low. In the numerical studies presented in Section 4, three possible definitions of means will be investigated:

$$
\overline{\eta} := \frac{1}{\text{no. of cells}} \sum_{K \in \mathcal{T}^h} \eta_K, \quad \text{the mean over all mesh cells, (mean)},
\tag{5}
$$

$$
\overline{\eta}^t := \frac{1}{\text{no. of time steps}} \sum_{\text{time steps}} \overline{\eta}, \quad \text{time average (mean\_time)},
\tag{6}
$$

$$
\overline{\eta}^{t/2} := \frac{\overline{\eta} + \overline{\eta}^t}{2}, \quad \text{linear combination, (mean\_mean)}.
\tag{7}
$$

Of course, considering time averages makes sense only if main features of the flow, like the inflow velocity, do not change much during the simulation. Another possibility for defining a time average would be the consideration of a prescribed number of last time steps instead of all time steps.

Four different types of turbulence regions will be considered. For very large η_K, $K \in \mathcal{T}^h$, the eddy viscosity model should be applied locally to all resolved scales. This corresponds to choosing $L^H(K)$ to be the space consisting only of the zero tensor, denoted by $P_{00}(K)$. Otherwise, $L^H(K)$ can be chosen to be $P_0(K)$, $P_1^{\text{disc}}(K)$, or $P_2^{\text{disc}}(K)$, corresponding to large, small and very small η_K, respectively. The superscript indicates that the global finite element space consists of discontinuous functions, the functions on each mesh cell are continuous. The choice $P_2^{\text{disc}}(K)$ corresponds to (almost) switching off the turbulence model. There are very few scales left in $\mathbb{D}(\mathbf{u}^h) - \mathbb{G}^H$ in this case. Since we think that the possibility of switching off the turbulence model should be available in the method, we set $\nu_T = 0$ in the case of very small η_K. In more detail, regarding the definition of the four turbulence regions, consider $C_1 \leqslant C_2 \leqslant C_3$, all non-negative, and denote by η the ratio between η_K and one of the means above, then $L^H(K)$ will be chosen as follows:

(1) for cells K with $\eta \leqslant C_1$: $L^H(K) = P_2^{\text{disc}}(K), \nu_T(K) = 0$,
(2) for cells K with $C_1 < \eta \leqslant C_2$: $L^H(K) = P_1^{\text{disc}}(K)$,
(3) for cells K with $C_2 < \eta \leqslant C_3$: $L^H(K) = P_0(K)$,
(4) for cells K with $C_3 < \eta$: $L^H(K) = P_{00}(K)$.

In the numerical simulations, together with the three different means, different values for C_1, C_2, C_3 will de studied.

Another parameter in the large-space-adaptive method is the number of time steps n_{update} after which the space L^H will be updated. This can be done after each time step but also after a prescribed number of time steps only. An update of L^H involves some additional numerical work, since some matrices, which would not change if L^H would stayed the same, have to be allocated and assembled again because of the changing dimension of L^H. In a discrete time t_k, updates of L^H are performed only at the beginning of the computations. For this reason, the adaptive choice of L^H is based on the finite element solution of the previous discrete time t_{k-1}.

The above criteria for locally choosing the large scale space is based on heuristic arguments. We are presently not aware of any results we could apply in order to mathematically support this choice. In the next section we will present the results of first numerical tests showing that the large-space-adaptive method with appropriately chosen parameters selects appropriate large scale spaces.

4. Numerical studies

We will consider two examples in the numerical studies, a strongly underresolved turbulent channel flow and a turbulent flow around a cylinder. The Q_2/P_1^{disc} pair of finite element spaces was used for velocity and pressure in all simulations presented below. This pair of finite elements is among the best performing ones for incompressible flow simulations [23,25,26]. All simulations were performed with the code MooNMD [27].

4.1. The turbulent channel flow at $Re_\tau = 180$

Turbulent channel flows are standard benchmark problems for turbulent flow simulations. These flows are statistically steady-state. The turbulent channel flow at $Re_\tau = 180$ was defined in [28] where also reference values for time and space-averaged flow quantities are given. The setup of this problem for the projection-based FEVMS method is presented in detail in [17].

The numerical studies at the turbulent channel flow should be considered as a proof of concept. Firstly, it will be shown that (4) gives appropriate information on the appearance of turbulence such that $L^H(K)$ is chosen in a way which can be expected. Secondly, the different possibilities (5)–(7) for defining a mean value of η_K will be studied, several choices of the parameters C_1, C_2, C_3 and the effect of the frequency of updating the space L^H, n_{update}, on the results of the large-space-adaptive method will be investigated. Comparisons with simulations with uniform spaces L^H will be presented as well.

The flow is given in $\Omega = (-2\pi,\ 2\pi) \times (0,\ 2) \times (-2\pi/3,\ 2\pi/3)$ with periodic boundary conditions in streamwise and spanwise direction. At the walls $y = 0$ and $y = 2$, no-slip boundary conditions are prescribed. We will consider this flow on a very coarse grid. This corresponds to a typical situation in applications where the grid size is often coarser by magnitudes than the size of the smallest scales. The grid consists of $8 \times 16 \times 8 = 1024$ mesh cells, which results in 25,344 velocity degrees of freedom and in 4096 pressure degrees of freedom. It is uniform in streamwise and spanwise direction but anisotropic in wall normal direction where the grid points are distributed accordingly to

$$y_i = 1 - \cos\left(\frac{i\pi}{16}\right), \quad i = 0, \ldots, 16.$$

As eddy viscosity model, we used the van Driest damping of the Smagorinsky model [3,29]

$$\nu_T = 0.01(2h_{K,\min})^2 \left\|\mathbb{D}(\mathbf{u}^h)\right\|_F \begin{cases} \left(1 - \exp\left(\frac{-y^+}{A}\right)\right)^2, & y^+ < 5, \\ 1 & \text{else}, \end{cases} \tag{8}$$

with $h_{K,\min}$ being the shortest edge of a mesh cell K, $\|\cdot\|_F$ being the Frobenius norm, $A = 26$ and $y^+ = Re_\tau y = 180y$ being the distance from the wall measured in wall units (or viscous lengths). All simulations started with a fully developed flow field. Initially, $L^H(K) = P_0(K)$ was chosen for all mesh cells. We allowed the simulations 10 (non-dimensionalized) time units to develop with the parameter (8) and the adaptive strategy for choosing L^H. The time-averages presented below were computed in another 30 (non-dimensionalized) time units. The Crank–Nicolson scheme was applied with the equidistant time step $\Delta t = 0.004$. This is smaller than the Kolmogorov time scale and it fits into the range of the time step proposed in [30]. Below, comparisons of the mean velocity profile U^h_{mean} and the rms turbulence intensity $u^{h,*}_{\text{rms}}$ with the data from [28] are given. The computed mean values are the average of the mean values of the lower and upper half of the channel. For details on the computations of these quantities, we refer to [17].

Besides the $L^2(K)$-norm of the resolved small scales (4), one could think that also the ratio of this norm to the $L^2(K)$-norm of all resolved scales

$$\eta^*_K = \frac{\|\mathbb{D}(\mathbf{u}^h) - \mathbb{G}^H\|_{L^2(K)}}{\|\mathbb{D}(\mathbf{u}^h)\|_{L^2(K)}}, \quad K \in \mathcal{T}^h, \tag{9}$$

might be an appropriate measure for the intensity of the local turbulence. In turbulent channel flows, a strong turbulence can be expected at the walls. Fig. 1 shows typical snapshots of spatial distributions with respect to the wall normal direction of (4) and (9). Each column in the pictures shows the values of all mesh cells with the respective y-coordinate of the bary center. The values of η_K at the walls, which are located at $y = 0$ and $y = 2$, are very large compared with the values in the center of the channel. In contrast, the values of η^*_K are rather equidistributed in the channel. Thus, it is possible to derive from (4) the correct information about the distribution of the local turbulence but not from (9).

We performed numerous simulations with different parameters in the large-space-adaptive method for choosing L^H. For shortness of presentation, only representative results are given below.

Results obtained with the definitions (5)–(7) of the mean values, for a fixed set of parameters C_1, C_2, C_3 and a fixed number of time steps $n_{\text{update}} = 10$ to update L^H, are presented in Fig. 2. In addition, results obtained with the fixed a priori choices $L^H = P_0$ (vms0) and $L^H = P_1^{\text{disc}}$ (vms1) are shown. It can be observed that there are only very slight differences in the curves with the different mean values. The rms turbulence intensity is overpredicted in all simulations. The overprediction of second order statistics is typically observed in turbulent channel flow simulations with low order discretizations like finite elements or finite volumes on coarse grids [17,21,31,32].

The choice of the parameters C_1 and C_2 has a much stronger effect on the results than the choice of the mean value, see Fig. 3. Generally, the large-space-adaptive method works the following way: the larger the values C_1, C_2, C_3, the larger the space L^H becomes and the less eddy viscosity is introduced into the simulations. The results presented in Fig. 3 show that in this example the values $C_1 \in \{0.2, 0.3\}$ and $C_2 \in \{0.5, 0.75\}$ lead to the best results. The value of C_3 has comparatively little influence. For $C_3 \geqslant 2$, the curves are almost identical if all other parameters in the simulations are chosen to be the same.

Fig. 4 presents results with different numbers of time steps between the updates of L^H. With respect to this parameter, there are only slight differences in the curves. This parameter plays for simulations of the statistically steady-state turbulent channel flow obviously a minor role.

Appropriate choices of the parameters in the large-space-adaptive method lead with respect to the mean velocity profile to somewhat more accurate results than both fixed choices of the large scale space. All results with the large-space-adaptive method are more accurate than the results with $L^H = P_1^{\text{disc}}$ with respect to $u^{h,*}_{\text{rms}}$.

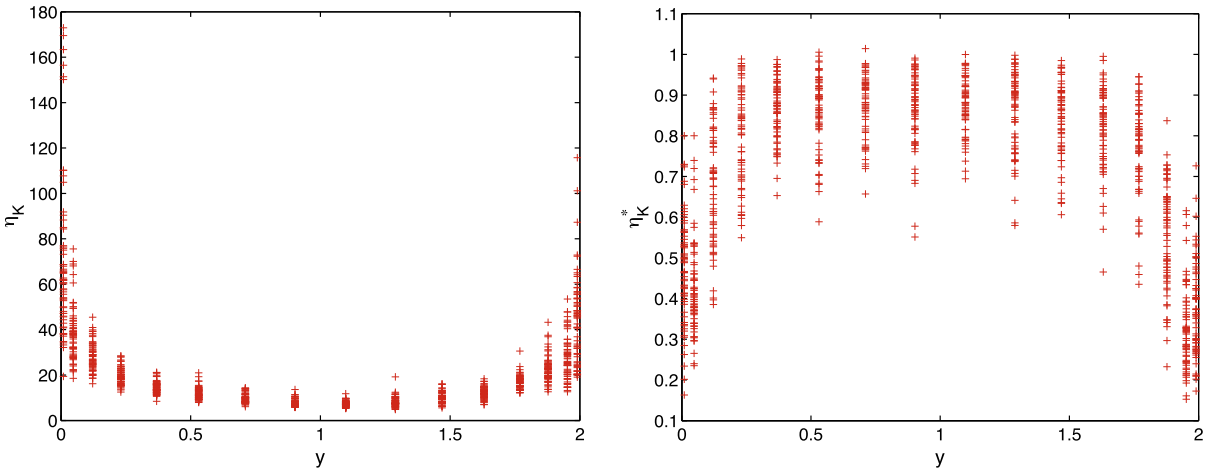

Fig. 1. Turbulent channel flow. Size of η_K computed with (4) (left) and size of (9) (right) in a simulation with $L^H = P_0$. The y-coordinate is the y-coordinate of the bary center of the mesh cells.

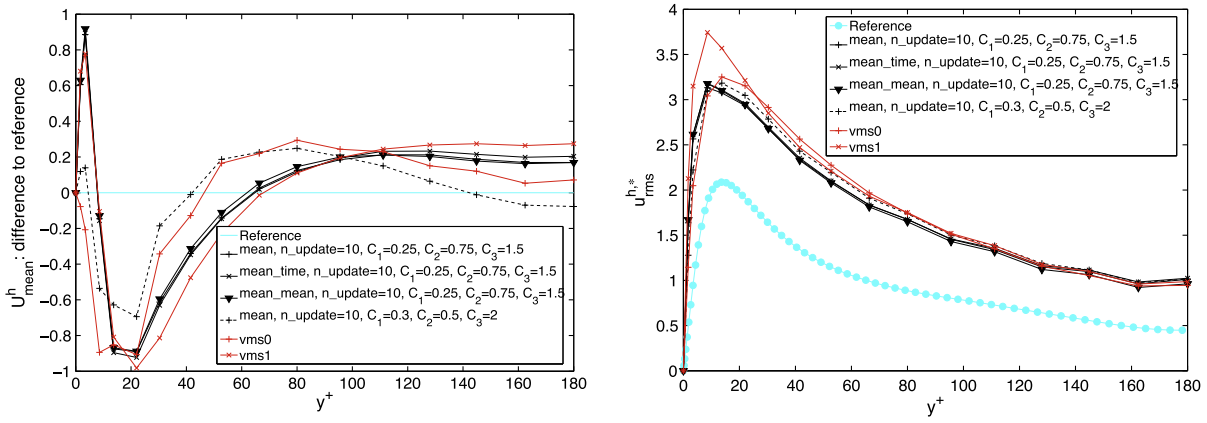

Fig. 2. Turbulent channel flow. Difference to the reference mean velocity and the rms intensities for using different methods for computing mean values in the adaptive method for choosing L^H.

Next, we like to illustrate the way the large scale space L^H is chosen with the large-space-adaptive method. Fig. 5 shows adaptively chosen spaces for two sets of parameters C_1, C_2, C_3. One can observe that at the walls locally small spaces were chosen for $L^H(K)$ whereas the eddy viscosity model was switched off in the center of the channel.

Finally, Fig. 6 illustrates the development of the size (number of degrees of freedom) of the space L^H for different parameters C_1, C_2, C_3 and n_{update}.

4.2. Turbulent flow around a cylinder with square cross-section at $Re = 22,000$

This example was defined in [33]. The flow domain and the initial grid (level 0) consisting of hexahedra are presented in Fig. 7. We performed the simulations on level 2, resulting in 522,720 velocity degrees of freedom and 81,920 pressure degrees of freedom. The inflow is prescribed by

$$\mathtt{u}(t,0,y,z) = (1 + 0.04\ \mathtt{rand}, 0, 0)^{\mathrm{T}},$$

where `rand` is a random number in $[-0.5, 0.5]$. The noise in the inflow serves to stimulate the turbulence. No-slip boundary conditions were prescribed at the column. Outflow boundary conditions were set at $x = 2.5$ m. On all other boundaries, free slip conditions were used. The Reynolds number of the flow, based on the mean inflow $U_\infty = 1$ m/s, the length of the cylinder $D = 0.1$ m and the viscosity $\nu = 1/220,000$ m^2/s is $Re = 22,000$. There are no external forces acting on the flow.

The Crank–Nicolson scheme was applied with equidistant time steps of length $\Delta t = 0.005$. Again, the Smagorinsky model with van Driest damping (8) was used as eddy viscosity model. Since we could not find in the literature values for u_τ to compute $y^+ = u_\tau y/\nu$, we performed as preprocessing step simulations with the FEVMS method with $L^H = P_0$ to get estimates for u_τ. We obtained $u_\tau = 2300$ for the front wall of the cylinder, $u_\tau = 1500$ for the lateral walls and $u_\tau = 1000$ for the back wall. These values were used in the van Driest damping model (8) for all simulations presented below.

This example describes a statistically periodic flow. Functionals of interest of the flow are the drag and the lift coefficient at the cylinder and the Strouhal number. The coefficients can be computed as volume integrals, e.g. see [8],

$$c_d(t) = -\frac{2}{\rho D H U_\infty^2}[(\mathbf{u}_t, \mathbf{v}_d) + (\nu\nabla\mathbf{u}, \nabla\mathbf{v}_d) + b(\mathbf{u},\mathbf{u},\mathbf{v}_d) - (p, \nabla\cdot\mathbf{v}_d)]$$

for any function $\mathbf{v}_d \in (H^1(\Omega))^3$ with $(\mathbf{v}_d)|_S = (1,0,0)^T$, where $\mathbf{v}_d$ vanishes on all other boundaries and S is the boundary of the cylinder. The density of the fluid is in this example $\rho = 1$ kg/m^3. Similarly, it holds

$$c_l(t) = -\frac{2}{\rho D H U_\infty^2}[(\mathbf{u}_t, \mathbf{v}_l) + (\nu\nabla\mathbf{u}, \nabla\mathbf{v}_l) + b(\mathbf{u},\mathbf{u},\mathbf{v}_l) - (p, \nabla\cdot\mathbf{v}_l)]$$

for any function $\mathbf{v}_l \in (H^1(\Omega))^3$ where $(\mathbf{v}_l)|_S = (0,1,0)^T$ and $\mathbf{v}_l$ vanishes on all other boundaries. Note, there is a jump in the definition of $\mathbf{v}_d$ and $\mathbf{v}_l$ at the upper and lower edges of the cylinder. However, using quadrature rules with interior quadrature points for the evaluation of $c_d(t)$ and $c_l(t)$, e.g. Gaussian quadrature, this inconsistency does not play any role in the computation of $c_d(t)$ and $c_l(t)$. The actual choice of $\mathbf{v}_d$ and $\mathbf{v}_l$ in our computations was the same as in [34]. The Strouhal number is defined by $St = DU_\infty/T$, where T is a characteristic time scale (the average length of a period in this example). Below, time-averaged drag and lift coefficients, $\bar{c}_d$ and $\bar{c}_l$, root mean squared (rms) values for c_d, c_l which are defined by

$$c_{d,\text{rms}} = \left(\sum_i (c_d(t_i) - \bar{c}_d)^2\right)^{1/2}, \quad c_{l,\text{rms}} = \left(\sum_i (c_l(t_i) - \bar{c}_l)^2\right)^{1/2},$$

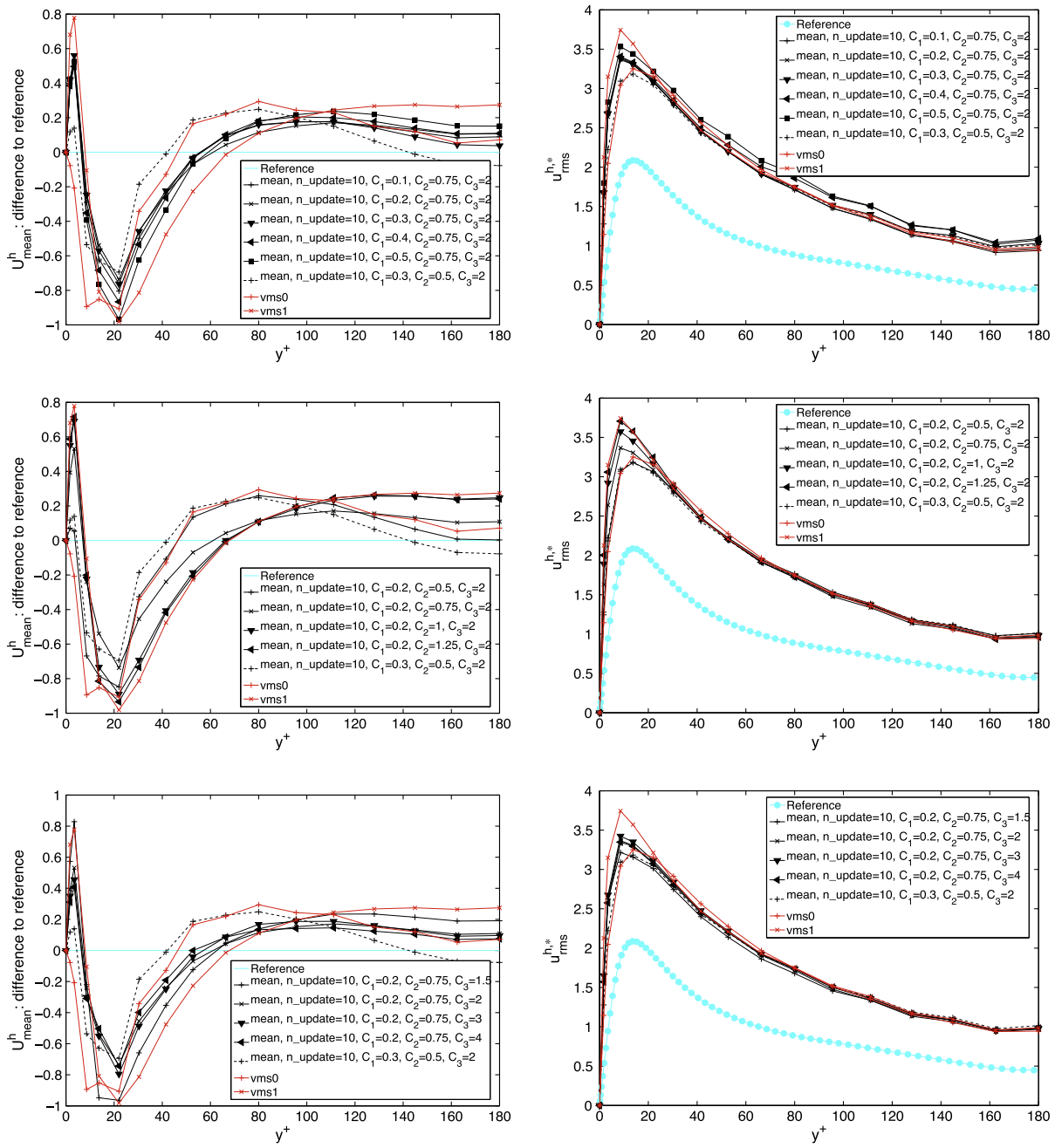

Fig. 3. Turbulent channel flow. Difference to the reference mean velocity and the rms intensities for using different sets of constants in the adaptive method for choosing L^H.

where the summation covers all discrete times in the time interval for which $\bar{c}_d, \bar{c}_l$ were computed, and the Strouhal number are presented.

All computations started with a fully developed flow field. After having allowed the flows 10 (non-dimensionalized) time units for developing with respect to the used method, the time averages were computed using the data of the following 30 full periods. The beginning of a period is defined by c_l changing from negative to positive values.

Results of our simulations are presented in Table 1. Experimental values, from [33], are given as comparison with the values obtained with the numerical simulations. One can observe that $\bar{c}_d$ is overpredicted in all simulations. This overprediction can already be seen for most codes in the comparative study from [33]. The value $\bar{c}_l$ is close to zero for all simulations. The predicted Strouhal numbers are often rather similar.

right: different numbers of time steps between the updates of L^H.

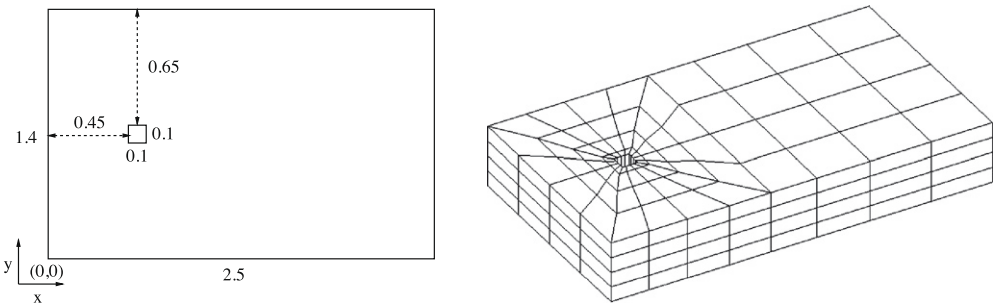

Fig. 7. Turbulent flow around a cylinder with square cross-section. Left: the cross-section of the domain (all length in m), the height of the channel is $H = 0.4$ m; right: initial grid.

Table 1
Turbulent flow around a cylinder with square cross-section. Time-averaged functionals of interest and corresponding rms values.

C_1	C_2	C_3	Mean	n_{update}	$\bar{c}_l$	$c_{l,\text{rms}}$	$\bar{c}_d$	$c_{d,\text{rms}}$	St
VMS with $L^H = P_0$					−0.002	0.96	2.48	0.15	0.139
VMS with $L^H = P_1^{\text{disc}}$					−0.015	0.97	2.42	0.17	0.137
0.2	0.5	2	$\bar{\eta}$	1	−0.006	1.30	2.54	0.18	0.137
0.2	0.75	2	$\bar{\eta}$	1	0.005	1.34	2.56	0.14	0.141
0.2	1	2	$\bar{\eta}$	1	0.007	1.14	2.48	0.18	0.136
0.2	1.25	2	$\bar{\eta}$	1	0.013	1.36	2.58	0.11	0.141
0.3	0.5	2	$\bar{\eta}$	1	−0.010	1.29	2.55	0.15	0.139
0.3	0.75	2	$\bar{\eta}$	1	−0.016	1.28	2.55	0.14	0.139
0.3	1	2	$\bar{\eta}$	1	0.004	1.27	2.53	0.13	0.137
0.3	1.25	2	$\bar{\eta}$	1	0.005	1.33	2.55	0.15	0.140
0.2	0.5	2	$\bar{\eta}$	10	0.004	1.35	2.57	0.12	0.140
0.2	0.75	2	$\bar{\eta}$	10	−0.002	1.26	2.52	0.16	0.138
0.2	1	2	$\bar{\eta}$	10	0.004	1.14	2.47	0.20	0.141
0.2	1.25	2	$\bar{\eta}$	10	−0.015	1.25	2.55	0.11	0.137
0.2	0.5	2	$\bar{\eta}^{t/2}$	1	−0.024	1.35	2.57	0.11	0.140
0.2	0.75	2	$\bar{\eta}^{t/2}$	1	−0.019	1.20	2.53	0.13	0.141
0.2	1	2	$\bar{\eta}^{t/2}$	1	−0.004	1.20	2.53	0.12	0.139
0.2	1.25	2	$\bar{\eta}^{t/2}$	1	−0.021	1.34	2.55	0.18	0.140
		Experiments				0.7–1.4	1.9–2.1	0.1–0.2	0.132

The most obvious difference between the FEVMS methods with uniform and with adaptive large scale space is in $c_{l,\text{rms}}$. Although all values are within the experimental range, the values obtained with the adaptive large scale space are in general notably larger.

Some other properties of the computed flow fields are presented in Figs. 8–10, where all averages were computed in the vertices of the mesh cells. One can observe that all results at the cylinder are rather similar, which comes from the small influence of the eddy viscosity model due to the van Driest damping. Concerning the large-space-adaptive FEVMS method, representative results are shown.

Fig. 8 presents the mean value of the first component of the velocity U along the center plane $y = 0.7$. It can be observed that negative streamwise velocities are computed in the nearest mesh point in front of the cylinder. The modulus of this value is considerably larger for the FEVMS methods with uniform large scale space. Behind the cylinder, the typical form of the curves is observed, as can be found e.g. in [33]. In particular, one can recognize that the choice of n_{update} has a major impact on the results downstream the cylinder.

Fig. 9 shows the averaged pressure distribution along the cylinder (front side at the beginning). The values were computed by averaging the discontinuous finite element pressure in the vertices of the mesh cells. The singularities of the pressure at the edges between the front and the lateral faces of the cylinder can be clearly seen. These singularities are somewhat larger for the FEVMS methods with adaptive large scale space. At the lateral sides and the back side, the pressure computed with the large-space-adaptive schemes is a little bit smaller than for the schemes with uniform large scale space.

The average of the first component of the velocity at the body, for $x = 0.5$, is presented in Fig. 10. The negative values at the lateral sides of the cylinder are somewhat larger for the schemes with adaptive large scale space. The FEVMS method with $L^H = P_0$ is the only method where the peak of the negative velocity is not in the nearest mesh point at the wall.

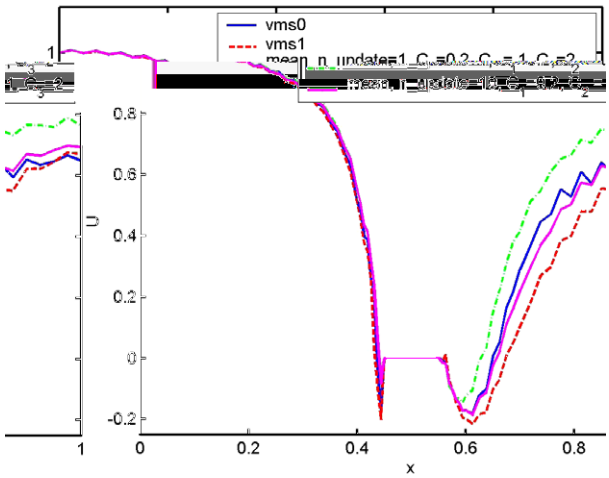

Fig. 8. Turbulent flow around a cylinder with square cross-section. Mean velocity distribution at the center plane $y = 0.7$.

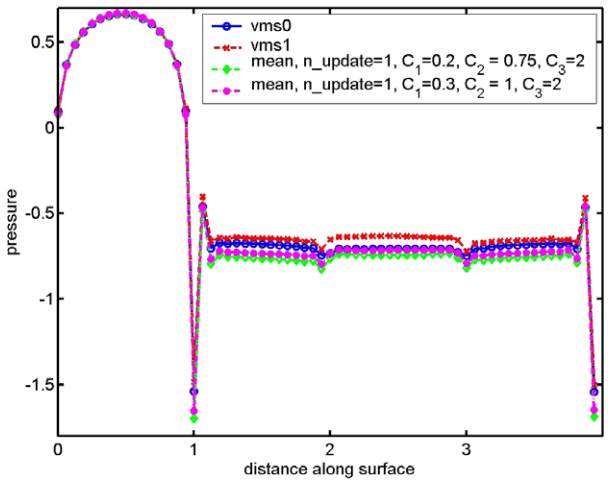

Fig. 9. Turbulent flow around a cylinder with square cross-section. Averaged pressure on the cylinder.

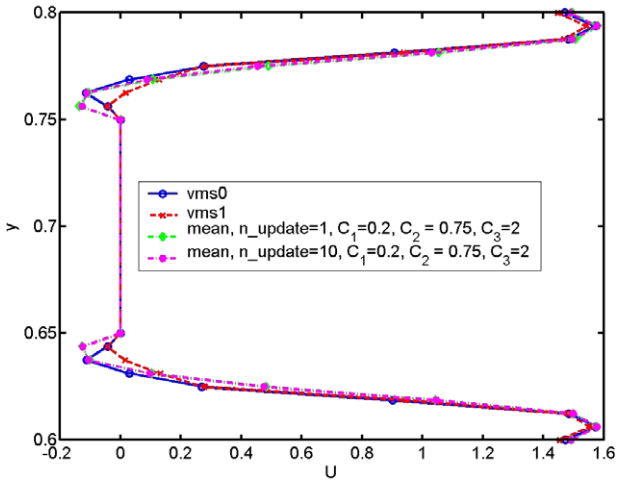

Fig. 10. Turbulent flow around a cylinder with square cross-section. Averaged streamwise velocity at the body for $x = 0.5$.

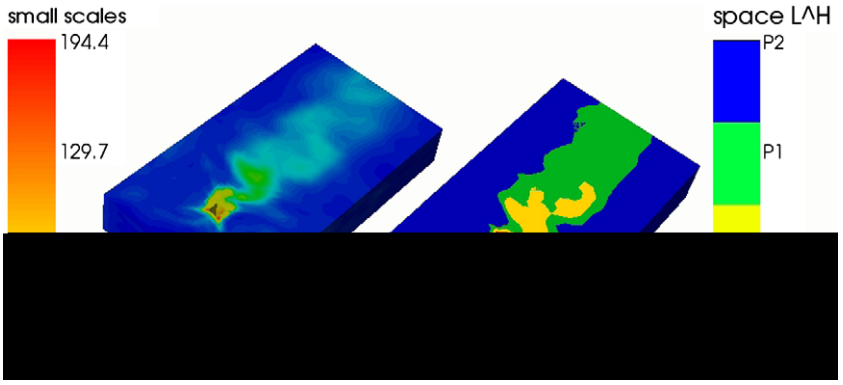

Fig. 11. Turbulent flow around a cylinder with square cross-section. Snapshot of η_K and L^H for $C_1 = 0.3, C_2 = 0.75$, $C_3 = 2, n_{\text{update}} = 1$ and the indicator $\bar{\eta}$.

Altogether, there are a number of choices for the parameters in the FEVMS method with adaptive large scale space which lead to satisfactory results. Some clear differences to the results of the methods with uniform large scale space can be observed.

A typical snapshot of the distribution of the resolved small scales and the corresponding space L^H is presented in Fig. 11. Also for the turbulent flow around a cylinder, the large scale space is chosen in such a way that the eddy viscosity model becomes effective only where turbulence occurs: at the cylinder and downstream the cylinder.

There are a number of open questions concerning the general relation between the parameters of the large-space-adaptive method and the computed quantities of interest. This situation emphasizes the need of a mathematical analysis of the method, which has to be started most probably at a much simpler example than the turbulent flow around a cylinder.

5. Summary and outlook

This paper presented a three-level finite element variational multiscale method for turbulent flow simulations with an adaptive choice of the large scale space. The large scale space L^H is chosen a posteriorly and it is allowed to posses a different polynomial degree in different mesh cells. The adaption is based on the size of the computed resolved small scales as local indicator of the amount of turbulence. Four parameters are contained in the algorithm for choosing the local space $L^H(K)$, a fifth parameter is introduced in the updating process.

The adaption criteria is a heuristic one. In order to test this choice, numerous simulations were performed for a turbulent channel flow and a turbulent flow around a cylinder, with different values for the parameters. In the snapshots in Figs. 5 and 11 it can be seen that the method chooses the large scale space in an appropriate way, i.e. the effect of the turbulence model is controlled by the adaptively chosen large scale space. Compared with choosing the same large scale space in all mesh cells and for all times, it could be seen that appropriate choices of parameters in the large-space-adaptive method often lead to improvements of the results. Thus, these first numerical results not only support our choice for the adaption criteria, but also show that the idea of adaptively choosing the large scale space is worthy of further investigations.

Regarding the parameters, in the case of the turbulent channel flow, we could observe only very small differences in the curves obtained with the different means (5)–(7). The choice of the parameters C_1 and C_2 had a much stronger influence on the results. The value of parameter C_3 had comparatively little influence, so did n_{update}, the number of time steps between the updates of L^H. The rms turbulence intensity was overpredicted in all simulations with the large-space-adaptive approach. With appropriate choices for the parameters, the approximation of the mean velocity profile was somewhat more accurate than in the simulations with a uniform large scale space. All approximations of $u_{\text{rms}}^{h,*}$ obtained with the FEVMS method with adaptive large scale space were better than the ones obtained with $L^H = P_1^{\text{disc}}$.

In the case of the turbulent flow around a cylinder, the numerical results showed a complex relation between the parameters of the large-space-adaptive FEVMS method and the computed quantities of interest, with a number of open questions left. With respect to a number of flow characteristics, similar results were obtained with the FEVMS methods with uniform large scale space and with adaptive large scale space for a wide range of parameters. The value of $\bar{c}_d$ was overpredicted in all simulations, all other values were in the experimental range. Notable differences to the FEVMS methods with uniform large scale space could be observed for $c_{l,\text{rms}}$.

The presented numerical studies give first guidelines on the importance of the parameters in the large-space-adaptive FEVMS method and their appropriate choice. Further studies, also at different flows, have to refine these guidelines. For a sound support of the adaption criteria and an appropriate choice of the parameters involved, a mathematical analysis of the method would be helpful.

References

[1] B. Mohammadi, O. Pironneau, Analysis of the K-Epsilon Turbulence Model, John Wiley & Sons, 1994.
[2] P. Sagaut, Large Eddy Simulation for Incompressible Flows, 3rd ed., Springer-Verlag, Berlin, Heidelberg, New York, 2006.
[3] L.C. Berselli, T. Iliescu, W.J. Layton, Mathematics of large eddy simulation of turbulent flows, Springer-Verlag, 2006.
[4] J.S. Smagorinsky, General circulation experiments with the primitive equations, Mon. Weather Rev. 91 (1963) 99–164.
[5] M. Germano, U. Piomelli, P. Moin, W. Cabot, A dynamic subgrid-scale eddy viscosity model, Phys. Fluids A 3 (1991) 1760–1765.
[6] D.K. Lilly, A proposed modification of the Germano subgrid-scale closure method, Phys. Fluids A 4 (1992) 633–635.
[7] A. Dunca, V. John, W.J. Layton, The commutation error of the space averaged Navier–Stokes equations on a bounded domain, in: J.G. Heywood, G.P. Galdi, R. Rannacher (Eds.), Contributions to Current Challenges in Mathematical Fluid Mechanics, Birkhäuser, 2004, pp. 53–78.
[8] V. John, Large eddy simulation of turbulent incompressible flows, in: Analytical and Numerical Results for a Class of LES Models, Lecture Notes in Computational Science and Engineering, vol. 34, Springer-Verlag, Berlin, Heidelberg, New York, 2004.
[9] L.C. Berselli, V. John, Asymptotic behavior of commutation errors and the divergence of the reynolds stress tensor near the wall in the turbulent channel flow, Math. Meth. Appl. Sci. 29 (2006) 1709–1719.
[10] L.C. Berselli, C.R. Grisanti, V. John, Analysis of commutation errors for functions with low regularity, J. Comp. Appl. Math. 206 (2007) 1027–1045.
[11] T.J.R. Hughes, Multiscale phenomena: Green's functions, the Dirichlet-to-Neumann formulation, subgrid-scale models, bubbles and the origin of stabilized methods, Comp. Meth. Appl. Mech. Eng. 127 (1995) 387–401.
[12] J.-L. Guermond, Stabilization of Galerkin approximations of transport equations by subgrid modeling, M2AN 33 (1999) 1293–1316.
[13] T.J. Hughes, L. Mazzei, K.E. Jansen, Large eddy simulation and the variational multiscale method, Comput. Visual Sci. 3 (2000) 47–59.
[14] T.J.R. Hughes, G. Scovazzi, L.P. Franca, Multiscale and stabilized methods, in: E. Stein, R. de Borst, T.J.R. Hughes (Eds.), Encyclopedia of Computational Mechanics, John Wiley & Sons, 2004.
[15] V. John, On large eddy simulation and variational multiscale methods in the numerical simulation of turbulent incompressible flows, Appl. Math. 51 (2006) 321–353.
[16] V. Gravemeier, The variational multiscale method for laminar and turbulent flow, Arch. Comput. Meth. Eng. 13 (2006) 249–324.
[17] V. John, M. Roland, Simulations of the turbulent channel flow at $Re_\tau = 180$ with projection-based finite element variational multiscale methods, Int. J. Numer. Meth. Fluids 55 (2007) 407–429.
[18] V. John, A. Kindl, Numerical studies of finite element variational methods for turbulent flow simulations, Comput. Meth. Appl. Mech. Eng., in press, doi:10.1016/j.cma.2009.01.010.
[19] V. John, S. Kaya, A finite element variational multiscale method for the Navier–Stokes equations, SIAM J. Sci. Comp. 26 (2005) 1485–1503.
[20] W.J. Layton, A connection between subgrid scale eddy viscosity and mixed methods, Appl. Math. Comput. 133 (2002) 147–157.
[21] V. John, A. Kindl, Variants of projection-based finite element variational multiscale methods for the simulation of turbulent flows, Int. J. Numer. Meth. Fluids 56 (2008) 1321–1328.
[22] V. John, S. Kaya, W. Layton, A two-level variational multiscale method for convection-dominated convection–diffusion equations, Comp. Meth. Appl. Math. Eng. 195 (2006) 4594–4603.
[23] V. John, Reference values for drag and lift of a two-dimensional time dependent flow around a cylinder, Int. J. Numer. Meth. Fluids 44 (2004) 777–788.
[24] V. John, G. Matthies, J. Rang, A comparison of time-discretization/linearization approaches for the time-dependent incompressible Navier–Stokes equations, Comput. Meth. Appl. Mech. Eng. 195 (2006) 5995–6010.
[25] P.M. Gresho, R.L. Sani, Incompressible Flow and the Finite Element Method, Wiley, Chichester, 2000.
[26] V. John, Higher order finite element methods and multigrid solvers in a benchmark problem for the 3D Navier–Stokes equations, Int. J. Numer. Meth. Fluids 40 (2002) 775–798.
[27] V. John, G. Matthies, MooNMD – a program package based on mapped finite element methods, Comput. Visual Sci. 6 (2004) 163–170.
[28] D.R. Moser, J. Kim, N.N. Mansour, Direct numerical simulation of turbulent channel flow up to $Re_\tau = 590$, Phys. Fluids 11 (1999) 943–945.
[29] E.R. van Driest, On turbulent flow near a wall, J. Aerospace Sci. 23 (1956) 1007–1011.
[30] H. Choi, P. Moin, Effects of the computational time step on numerical solutions of turbulent flow, J. Comput. Phys. 113 (1994) 1–4.
[31] V. Gravemeier, Scale-separating operators for variational multiscale large eddy simulation of turbulent flows, J. Comput. Phys. 212 (2006) 400–435.
[32] V. Gravemeier, A consistent dynamic localization model for large eddy simulation of turbulent flows based on a variational formulation, J. Comput. Phys. 218 (2006) 677–701.
[33] W. Rodi, J.H. Ferziger, M. Breuer, M. Pourquié, Status of large eddy simulation: results of a workshop, J. Fluids Eng. 119 (1997) 248–262.
[34] V. John, G. Matthies, Higher order finite element discretizations in a benchmark problem for incompressible flows, Int. J. Numer. Meth. Fluids 37 (2001) 885–903.